An Electrochemical Ethylamine/Acetonitrile Redox Method for Ambient Hydrogen Storage

Authors: Dezhen Wu[1]†, Jialu Li[1]†, Libo Yao[1], Rongxuan Xie[1], and Zhenmeng Peng[1]*

Affiliations:

[1]Department of Chemical, Biomolecular, and Corrosion Engineering, The University of Akron; Akron, OH, 44325, United States.

*Corresponding author. Email: zpeng@uakron.edu

Abstract: Hydrogen storage presents a major difficulty in the development of hydrogen economy. Herein, we report a new electrochemical ethylamine/acetonitrile redox method for hydrogen storage with an 8.9 wt.% theoretical storage capacity under ambient conditions. This method exhibits low onset overpotentials of 0.19 V in $CH_3CH_2NH_2$ dehydrogenation to CH_3CN and 0.09 V in CH_3CN hydrogenation to $CH_3CH_2NH_2$ using commercial Pt black catalyst. By assembling a full cell that couples $CH_3CH_2NH_2$/CH_3CN redox reactions with hydrogen evolution and oxidation reactions, we demonstrate a complete hydrogen storage cycle at fast rates, with only 52.5 kJ/mol energy consumption for H_2 uptake and release at a rate of 1 L/m^2·h. This method provides a viable hydrogen storage strategy that meets the 2025 Department of Energy onboard hydrogen storage target.

One-Sentence Summary: A new electrochemical ethylamine/acetonitrile redox method is reported to achieve efficient, high-capacity hydrogen storage with fast uptake and release rate and low energy consumption under ambient conditions.

Main Text: Hydrogen is an appealing energy carrier that can potentially replace conventional fossil fuels in the development of a clean, sustainable hydrogen economy, which would resolve environmental problems caused by the combustion of the non-renewable resources while also meeting the rising demand for energy (*1*, *2*). However, hydrogen storage has remained a major roadblock in the hydrogen economy development. Currently, hydrogen is mainly stored in the form of either compressed gas or cryogenic liquid. These methods are ill-suited for commercial applications due to their insufficient energy storage density (*3*). To make matters worse, extreme storage conditions are required, which not only result in a significant increment of the cost but also raise safety concerns (*3*). As a matter of fact, the state-of-the-art methods fall short of the 2025 Department of Energy (DOE) onboard hydrogen storage target of 5.5 wt.% under 85 °C and 12 bar.

To overcome these challenges, there have been extensive research efforts to discover alternative hydrogen storage methods in the past few decades. The developed methods can be primarily classified into two categories, i.e., physisorption and chemical conversion, depending on the storage mechanisms. The physisorption methods use large-surface, light-weight storage materials, which can weakly adsorb hydrogen molecules to their surface via the Van der Waals attraction force (*3*). Although many promising materials have been carefully investigated, such as carbon nanotubes (*4*, *5*), zeolites (*6*, *7*), metal organic frameworks (MOFs) (*8*, *9*), and covalent organic frameworks (COFs) (*10*), only a relatively low storage capacity (typically less than 1~2 wt.%) can be obtained, even under their best preformed low temperature and high pressure conditions (*11*). The chemical conversion methods involve uptake of hydrogen by storage materials via hydrogenation and release of hydrogen via decomposition. A range of chemical compounds, for instance, aluminum and magnesium hydrides (*12*, *13*), metal complex hydrides (*14*), and amides/imides (*15*), have been considered as promising candidates and extensively studied. Many of these chemical compounds possess >5.5 wt.% theoretical hydrogen uptake/release that exceeds the DOE goal of storage capacity. However, to date, none of them have been able to meet the DOE goals regarding operation conditions and cost. This is because these chemical hydrogen storage processes generally go through complex reaction pathways with a high energy barrier. Furthermore, either the hydrogen uptake or release reaction would be endothermic from a thermodynamics point of view. Extremely high temperature and pressure conditions were thus required to complete a hydrogen storage cycle in these previous studies (*3*).

In this work, we report a new, electrochemical ethylamine/acetonitrile redox method for efficient, high-capacity hydrogen storage under completely ambient conditions. The amine/nitrile redox couple is selected due to their moderate chemical polarity and relatively simple hydrogenation and dehydrogenation pathways, which would aid reaction activation and reduce the energy barrier. Electrochemical potential provides the driving force in $CH_3CH_2NH_2$ dehydrogenation under ambient conditions, rather than high temperature and pressure that are typically required to thermally drive an endothermic process. We demonstrate an effective, complete cycle of CH_3CN hydrogenation to $CH_3CH_2NH_2$ for hydrogen uptake and $CH_3CH_2NH_2$ dehydrogenation to CH_3CN for hydrogen release at low overpotentials, using commercial Pt black catalyst in an electrochemical cell. The studied $CH_3CH_2NH_2/CH_3CN$ system has a theoretical H_2 storage capacity of 8.9 wt.%, well surpassing the 5.5 wt.% DOE target. This study offers a new, effective hydrogen storage strategy that can be extended to many other amine/nitrile redox systems and would help advance the hydrogen economy development.

Results and discussion

The electrochemical conversion between $CH_3CH_2NH_2$ and CH_3CN in an alkaline aqueous electrolyte occurs via a four-electron transfer dehydrogenation/hydrogenation process and exhibits a standard redox potential of 0.13 V vs. RHE (Fig. 1a). The reaction properties were studied by conducting electrochemical measurements under half-cell test condition, with the working electrode loaded with commercial Pt black catalyst for promoting the kinetics. Fig. 1b and S1 show cyclic voltammetry (CV) and linear sweep voltammetry (LSV) data collected in different electrolytes. In an 1M $CH_3CH_2NH_2$ + 1M NaOH electrolyte, the CV curve exhibited cathodic currents below 0 V, which corresponded to hydrogen evolution reaction (HER), and anodic currents above 0.32 V, which was attributed to $CH_3CH_2NH_2$ electrochemical oxidation because the anodic currents became negligible with the absence of $CH_3CH_2NH_2$ in the electrolyte. Proton nuclear magnetic resonance (^{1}H NMR) spectroscopy characterizations of the reacted solution found CH_3CN to be the only liquid product (Fig. 1c), confirming effective, selective $CH_3CH_2NH_2$ dehydrogenation to CH_3CN. The measured low onset overpotential of about 0.19 V suggested a fast dehydrogenation kinetics. This could benefit from a moderate polarity and basicity of amine molecules, which would allow for efficient activation towards electrochemical oxidation (*16*, *17*). The occurrence of $CH_3CH_2NH_2$ dehydrogenation on the working electrode was accompanied by HER on the counter electrode, as evidenced by mass spectrometry (MS) detection of H_2 product in the gas phase (Fig. 1d).

With the addition of CH_3CN to the electrolyte, the CV curve showed more significant cathodic currents below 0 V vs. RHE. Moreover, there was a slight positive shift in the onset potential to 0.04 V. These results suggested the occurrence of CH_3CN electrochemistry with an onset overpotential of 0.09 V, besides HER. ^{1}H NMR spectrum of the reaction product showed $CH_3CH_2NH_2$ as a major product and minor fractions of $(CH_3CH_2)_2NH$ and $(CH_3CH_2)_3N$ side products (Fig. 1e) (*18*, *19*). This confirmed CH_3CN can be effectively converted to $CH_3CH_2NH_2$ via electrochemical hydrogenation. It is worth noting that the CH_3CN hydrogenation efficiency and selectivity can be further improved by catalyst research. For instance, Zhang et al. reported a complete prevention of amine dimers and trimers formation and suppression of HER in CH_3CN hydrogenation to $CH_3CH_2NH_2$ using a Cu catalyst (*19*). Xia et al. investigated several catalyst materials in CH_3CN hydrogenation and found composition effects on the reaction activity and selectivity properties (*18*).

The effects of electrolyte pH and concentration on both $CH_3CH_2NH_2$ dehydrogenation and CH_3CN hydrogenation reaction properties were investigated. The highest current density for $CH_3CH_2NH_2$ dehydrogenation was obtained with 0.5 M NaOH, suggesting the optimal pH for this reaction (Fig. S2 and S3). With an increase in the $CH_3CH_2NH_2$ concentration, there was an improvement in the dehydrogenation rate together with a suppression in HER (Fig. S4 - S6). This can be explained by strong adsorption of amino groups to Pt catalyst (*16*, *17*), with which a higher concentration of $CH_3CH_2NH_2$ would lead to more active sites being occupied for its dehydrogenation and less active sites for HER. Chronoamperometry experiments at 0.5 V vs. RHE show time dependency of the current density (Fig. S7), which had a drastic decrease at the beginning and became more stabilized thereafter. The negligible influence of electrode rotation rate on the $CH_3CH_2NH_2$ dehydrogenation indicated minimal mass transfer limitation for this reaction under the studied condition (Fig. S8). For the reverse CH_3CN hydrogenation reaction, a higher current density was obtained with an increase in the pH and a decrease in CH_3CN concentration (Fig. S9 and S10). Because CH_3CN hydrogenation and HER occur simultaneously in the same potential region, there would be an interplay between the two processes that led to the observed changes. While the electrode rotation rate did not show a significant effect on the current density in CH_3CN hydrogenation region, it considerably affected the current density in

the positive potential range that corresponded to hydrogen oxidation reaction (HOR), particularly when the electrolyte was saturated with H_2 (Fig. S11). This was consistent with previous HOR studies and was attributed to a mass transfer limitation in this reaction (*20*).

The temperature effect on the two half-cell reactions were studied by measuring the LSV change with temperature, which was used for evaluating the reaction activity property (Fig. S12 and S13). Fig. 1f shows the obtained Arrhenius plot, which determined an apparent activation energy (E_a) value of 52.4 kJ/mol at 0.5 V vs. RHE for $CH_3CH_2NH_2$ dehydrogenation and 11.6 kJ/mol at -0.05 V vs. RHE. Although the latter accounted for CH_3CN hydrogenation with a mix of HER, these low E_a values revealed the rapid reaction kinetics and agreed well with the observed low overpotentials in $CH_3CH_2NH_2$ dehydrogenation and CH_3CN hydrogenation. Benefiting from their low activation energy, a minimal increase in the potential difference between the two half-cell reactions is needed to drastically improve the reaction current density (Fig. 1g), implying feasibility of utilizing these two reactions to realize energy-efficient, complete cycle of hydrogen storage.

Figure 2a illustrated the blueprint for a sustainable hydrogen economy, in which the electrochemical $CH_3CH_2NH_2/CH_3CN$ redox method plays a crucial role for hydrogen storage that bridges hydrogen production and various applications. The great potential of this new method was demonstrated by assembling a custom-made 10 cm^2 electrochemical cell and investigating the overall hydrogenation/dehydrogenation process to simulate a complete H_2 uptake/release cycle (Fig. S14). In H_2 uptake experiments, CH_3CN and H_2 were fed to the cathode and anode, at which CH_3CN hydrogenation and HOR occurred with an applied cell voltage (Fig. S15). Fig. 2b shows chronoamperometry tests of the cell at different voltages and the corresponding H_2 uptake performances. A notable current was measured even with a low cell voltage of 0.1 V. Except for the initial drop due to the capacitive current effect, the cell maintained a consistent current of roughly 6 mA throughout the experiment, indicating good durability for CH_3CN hydrogenation and HOR reactions. An increase in the cell voltage led to enhancements in the H_2 uptake rate. This was evidenced by the measured current and the $CH_3CH_2NH_2$ generation rate quantified with NMR analysis (Fig. S16), with $CH_3CH_2NH_2$ being produced at as high as 93.1 $mmol/m^2 \cdot h$ rate at 0.3 V. With increasing cell voltage, the faradaic efficiency for $CH_3CH_2NH_2$ production gradually increased, reaching about 60% at 0.3 V. The non-superior $CH_3CH_2NH_2$ faradaic efficiency was caused by side reactions including HER and generation of $(CH_3CH_2)_2NH$ and $(CH_3CH_2)_3N$ minor products, which was in agreement with the results under half-cell condition and can be improved by applying a more suitable catalyst(*18*, *19*). For H_2 release, $CH_3CH_2NH_2$ was fed to the anode and dehydrogenated to CH_3CN with an applied cell voltage (Fig. S17). This was coupled with HER at the cathode, transforming the hydrogen stored in $CH_3CH_2NH_2$ molecules to H_2 gas. Fig. 2c shows CV and chronoamperometry results of the cell, with H_2 generation being continuously measured using on-line mass spectroscopy (MS) (Fig. S18-S19). The H_2 generation became significant once the cell voltage turned positive, with the generation rate increasing rapidly with the voltage and the faradaic efficiency determined to be close to 100%. This was consistent with the finding of CH_3CN as the only liquid product and H_2 as the only gas product, confirming an excellent selectivity in H_2 release via $CH_3CH_2NH_2$ dehydrogenation. The cell durability was evaluated by conducting chronoamperometry experiments at different voltages. The current showed a rapid drop in the first few minutes and then became steadier throughout the remaining experiment with a constant voltage being applied (Fig. S20), suggesting promising cell durability. The current decayed more rapidly when the voltage was periodically turned on and off for simulating cell startup and shutdown operations (Fig. 2c), and the decay became more substantial as the voltage increased

(Fig. S21 and S22). This was likely due to a gradual deactivation of the Pt black catalyst under these stability test conditions. Regardless of the cell voltage, the faradaic efficiency was consistently greater than 94% and exhibited no signs of decrease.

We conducted an energy consumption analysis using the cell LSV data to assess the technical feasibility of this new electrochemical $CH_3CH_2NH_2$/ CH_3CN redox method for hydrogen storage application. Fig. 3a shows the measured cell I-V plots during H_2 uptake and release processes as well as the calculated power consumption in the individual steps, based on which the total energy consumption to complete a hydrogen storage cycle at any designated hydrogen uptake and release rate was computed (Fig. 3b). It appeared that the energy consumption per mole of H_2 for a complete storage cycle was a function of H_2 uptake and release rate, with extremely low energy consumption at slow rates. For instance, the H_2 uptake and release at a rate of 1 $L/m^2 \cdot h$ required only 52.5 kJ/mol energy consumption, which was dramatically smaller compared to 286 kJ/mol energy generation when the stored H_2 is combusted for application, suggesting the energy-efficient nature of the electrochemical $CH_3CH_2NH_2/CH_3CN$ redox method. Additionally, the hydrogen uptake/release temperature and pressure conditions should also be taken into account for cost and safety concerns. Although certain metal hydrides can achieve a high storage capacity, for instance, 7 wt.% for MgH_2 and 10 wt.% for AlH_3 (*21–25*), their hydrogen uptake/release process requires either >300 °C temperature or >20 bar pressure, if not both (Fig. 3c). A very recent study by Liu et al. reported a new multi-layered Ti_2CT_x material with 8.8 wt.% storage capacity at 60 bar, but achieving only 4 wt.% under ambient conditions (*26*). It is unprecedented that the electrochemical $CH_3CH_2NH_2/CH_3CN$ redox method is capable of completing a hydrogen uptake and release cycle with 8.9 wt.% storage capacity under entirely ambient conditions. To the best of our knowledge, this new method is the only approach that meets the 2025 DOE onboard hydrogen storage target in terms of storage capacity (≥5.5 wt.%), max delivery temperature (≤85 °C), and max delivery pressure (≤12 bar).

Conclusion

In summary, a novel electrochemical $CH_3CH_2NH_2/CH_3CN$ redox method was studied for ambient H_2 storage, which utilized electrochemical conversion between the two chemicals. The $CH_3CH_2NH_2$ dehydrogenation to CH_3CN using a commercial Pt black catalyst exhibited a low onset overpotential of 0.19 V, a moderate activation energy of 52.4 kJ/mol at 0.5 V vs. RHE, and produced CH_3CN as the only product, indicating fast reaction kinetics and excellent selectivity. The rapid CH_3CN hydrogenation to $CH_3CH_2NH_2$ was also evidenced by a low onset overpotential of 0.09 V and a low activation energy of 11.6 kJ/mol at -50 mV vs. RHE. A complete hydrogen uptake and release cycle was demonstrated with full cell testing, with 93.14 $mmol/m^2 \cdot h$ $CH_3CH_2NH_2$ generation rate and 60% faradaic efficiency for H_2 uptake at 0.3 V cell voltage, and 0.34 $mol/m^2 \cdot h$ H_2 generation rate and >94% faradaic efficiency for H_2 release at 0.4 V cell voltage. It is worth mentioning these results were obtained in a simply assembled electrochemical cell using commercial Pt black catalyst, implying the H_2 uptake and release rate as well as the faradaic efficiency can be further improved with cell engineering and new catalyst research. With 8.9 wt.% theoretical H_2 storage capacity, ambient reaction conditions, and 52.5 kJ/mol low energy consumption for H_2 uptake and release at a rate of 1 $L/m^2 \cdot h$, this study demonstrated the $CH_3CH_2NH_2/CH_3CN$ redox method as a viable hydrogen storage strategy that would contribute to advancing the hydrogen economy development.

References and Notes

1. G. W. Crabtree, M. S. Dresselhaus, M. V Buchanan, The hydrogen economy. *Phys.*

Today. **57**, 39–44 (2004).

2. S. S. Penner, Steps toward the hydrogen economy. *Energy*. **31**, 33–43 (2006).
3. P. Jena, Materials for hydrogen storage: Past, present, and future. *J. Phys. Chem. Lett.* **2**, 206–211 (2011).
4. Dillon, A., Jones, K., Bekkedahl, T. *et al.* Storage of hydrogen in single-walled carbon nanotubes. *Nature* **386,** 377–379 (1997).
5. P. Chen, X. Wu, J. Lin, K. L. Tan, High H_2 uptake by alkali-doped carbon nanotubes under ambient pressure and moderate temperatures. *Science.* **285**, 91–93 (1999).
6. J. Weitkamp, M. Fritz, S. Ernst, in *Proceedings from the ninth international zeolite conference* (Elsevier, 1993), pp. 11–19.
7. J. Dong, X. Wang, H. Xu, Q. Zhao, J. Li, Hydrogen storage in several microporous zeolites. *Int. J. Hydrogen Energy*. **32**, 4998–5004 (2007).
8. S. S. Kaye, A. Dailly, O. M. Yaghi, J. R. Long, Impact of preparation and handling on the hydrogen storage properties of Zn_4O (1, 4-benzenedicarboxylate) 3 (MOF-5). *J. Am. Chem. Soc.* **129**, 14176–14177 (2007).
9. J. Yang, A. Grzech, F. M. Mulder, T. J. Dingemans, Methyl modified MOF-5: a water stable hydrogen storage material. *Chem. Commun.* **47**, 5244–5246 (2011).
10. Z. Ke, Y. Cheng, S. Yang, F. Li, L. Ding, Modification of COF-108 via impregnation/functionalization and Li-doping for hydrogen storage at ambient temperature. *Int. J. Hydrogen Energy*. **42**, 11461–11468 (2017).
11. S. Niaz, T. Manzoor, A. H. Pandith, Hydrogen storage: Materials, methods and perspectives. *Renew. Sustain. Energy Rev.* **50**, 457–469 (2015).
12. C. M. Jensen, K. J. Gross, Development of catalytically enhanced sodium aluminum hydride as a hydrogen-storage material. *Appl. Phys. A*. **72**, 213–219 (2001).
13. P. de Rango, P. Marty, D. Fruchart, Hydrogen storage systems based on magnesium hydride: from laboratory tests to fuel cell integration. *Appl. Phys. A*. **122**, 1–20 (2016).
14. M. B. Ley, L. H. Jepsen, Y.-S. Lee, Y. W. Cho, J. M. B. Von Colbe, M. Dornheim, M. Rokni, J. O. Jensen, M. Sloth, Y. Filinchuk, Complex hydrides for hydrogen storage–new perspectives. *Mater. Today*. **17**, 122–128 (2014).
15. W. I. F. David, M. O. Jones, D. H. Gregory, C. M. Jewell, S. R. Johnson, A. Walton, P. P. Edwards, A mechanism for non-stoichiometry in the lithium amide/lithium imide hydrogen storage reaction. *J. Am. Chem. Soc.* **129**, 1594–1601 (2007).
16. A. Adenier, M. M. Chehimi, I. Gallardo, J. Pinson, N. Vilà, Electrochemical oxidation of aliphatic amines and their attachment to carbon and metal surfaces. *Langmuir*. **20**, 8243–8253 (2004).
17. J. Ghilane, P. Martin, H. Randriamahazaka, J. C. Lacroix, Electrochemical oxidation of primary amine in ionic liquid media: Formation of organic layer attached to electrode surface. *Electrochem. commun.* **12**, 246–249 (2010).
18. R. Xia, D. Tian, S. Kattel, B. Hasa, H. Shin, X. Ma, J. G. Chen, F. Jiao, Electrochemical reduction of acetonitrile to ethylamine. *Nat. Commun.* **12**, 1–8 (2021).

19. D. Zhang, J. Chen, Z. Hao, L. Jiao, Q. Ge, W.-F. Fu, X.-J. Lv, Highly efficient electrochemical hydrogenation of acetonitrile to ethylamine for primary amine synthesis and promising hydrogen storage. *Chem Catal.*, 1–14 (2021).

20. M. E. Scofield, Y. Zhou, S. Yue, L. Wang, D. Su, X. Tong, M. B. Vukmirovic, R. R. Adzic, S. S. Wong, Role of chemical composition in the enhanced catalytic activity of Pt-based alloyed ultrathin nanowires for the hydrogen oxidation reaction under alkaline conditions. *ACS Catal.* **6**, 3895–3908 (2016).

21. J. Huot, G. Liang, S. Boily, A. Van Neste, R. Schulz, Structural study and hydrogen sorption kinetics of ball-milled magnesium hydride. *J. Alloys Compd.* **293**, 495–500 (1999).

22. L. Wang, A. Rawal, K.-F. Aguey-Zinsou, Hydrogen storage properties of nanoconfined aluminium hydride (AlH_3). *Chem. Eng. Sci.* **194**, 64–70 (2019).

23. J. Graetz, B. C. Hauback, Recent developments in aluminum-based hydrides for hydrogen storage. *MRS Bull.* **38**, 473–479 (2013).

24. Y. Chen, C.-Z. Wu, P. Wang, H.-M. Cheng, Structure and hydrogen storage property of ball-milled $LiNH_2/MgH_2$ mixture. *Int. J. Hydrogen Energy*. **31**, 1236–1240 (2006).

25. Z. Xiong, G. Wu, J. Hu, P. Chen, Ternary imides for hydrogen storage. *Adv. Mater.* **16**, 1522–1525 (2004).

26. S. Liu, J. Liu, X. Liu, J. Shang, L. Xu, R. Yu, J. Shui, Hydrogen storage in incompletely etched multilayer Ti_2CTx at room temperature. *Nat. Nanotechnol.* **16**, 331–336 (2021).

Acknowledgments:

Funding:

The University of Akron, US

Author contributions:

D. Z. Wu† and J. L. Li† contributed equally to this work. D. Z. Wu designed and performed the half-cell experiments, analyzed the data and prepared the manuscript. J. L. Li conducted the full cell assembling, calibration and testing, and characterization of the reaction products. L. B. Yao and R. X. Xie contributed to full cell assembling and testing and results discussion. Z. M. Peng conceived the project, designed the experiments, and edited the manuscript.

Competing interests:

Authors declare that they have no competing interests.

Data and materials availability:

All data are available in the main text or the supplementary materials.

Supplementary Materials

Materials and Methods
Fig.S1~S13. Electrochemical measurements under half-cell conditions.

Fig. S14. Photos of the assembled electrochemical full cell.
Fig. S15, 17, 20~22. Electrochemical measurements under half-cell conditions.
Fig. S16 NMR characterization results.
Fig. S18~19. MS characterization and data calibration.

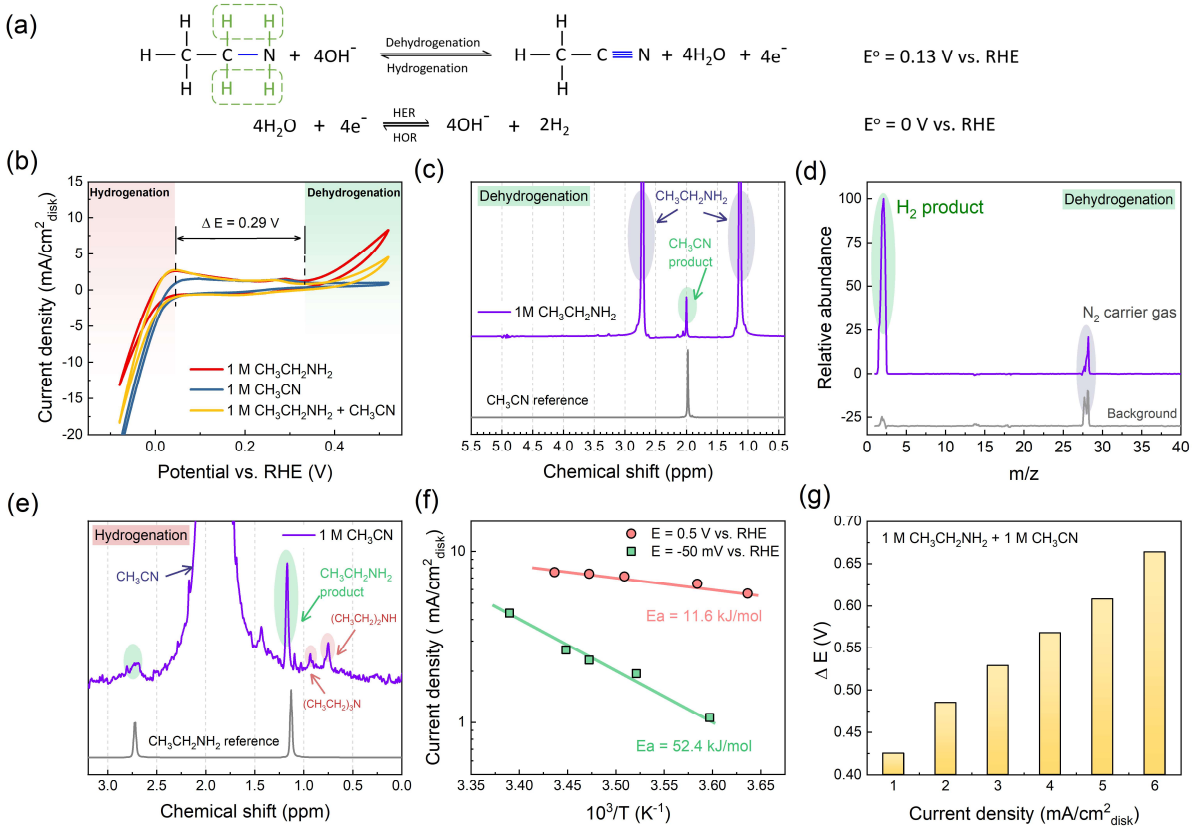

Fig. 1. Experimental measurements of electrochemical $CH_3CH_2NH_2/CH_3CN$ redox properties in alkaline aqueous electrolyte under half-cell condition. (a) Equation and standard potential for electrochemical $CH_3CH_2NH_2/CH_3CN$ redox reactions and hydrogen evolution and oxidation reactions under alkaline aqueous condition; (b) Cyclic voltammetry of commercial Pt black catalyst-loaded working electrode in 1 M NaOH aqueous solution with the addition of 1 M $CH_3CH_2NH_2$, 1 M CH_3CN, and 1 M $CH_3CH_2NH_2$ + 1 M CH_3CN, respectively; (c) ^1H NMR spectrum of liquid product from $CH_3CH_2NH_2$ dehydrogenation obtained by applying 0.7 V vs. RHE for 10 hours, with CH_3CN as a reference and (d) mass spectrum of gas product from the counter electrode in $CH_3CH_2NH_2$ dehydrogenation experiment; (e) ^1H NMR spectrum of liquid product from CH_3CN hydrogenation obtained by applying -0.4 V vs. RHE for 10 hours, with $CH_3CH_2NH_2$ as a reference; (f) Arrhenius plots obtained at 0.5 V vs. RHE in $CH_3CH_2NH_2$ dehydrogenation experiments and at -50 mV vs. RHE in CH_3CN hydrogenation experiments; (g) Potential difference between $CH_3CH_2NH_2$ dehydrogenation reaction and

CH_3CN hydrogenation reaction as a function of current density in 1 M NaOH aqueous solution with the addition of 1 M $CH_3CH_2NH_2$ and 1 M CH_3CN.

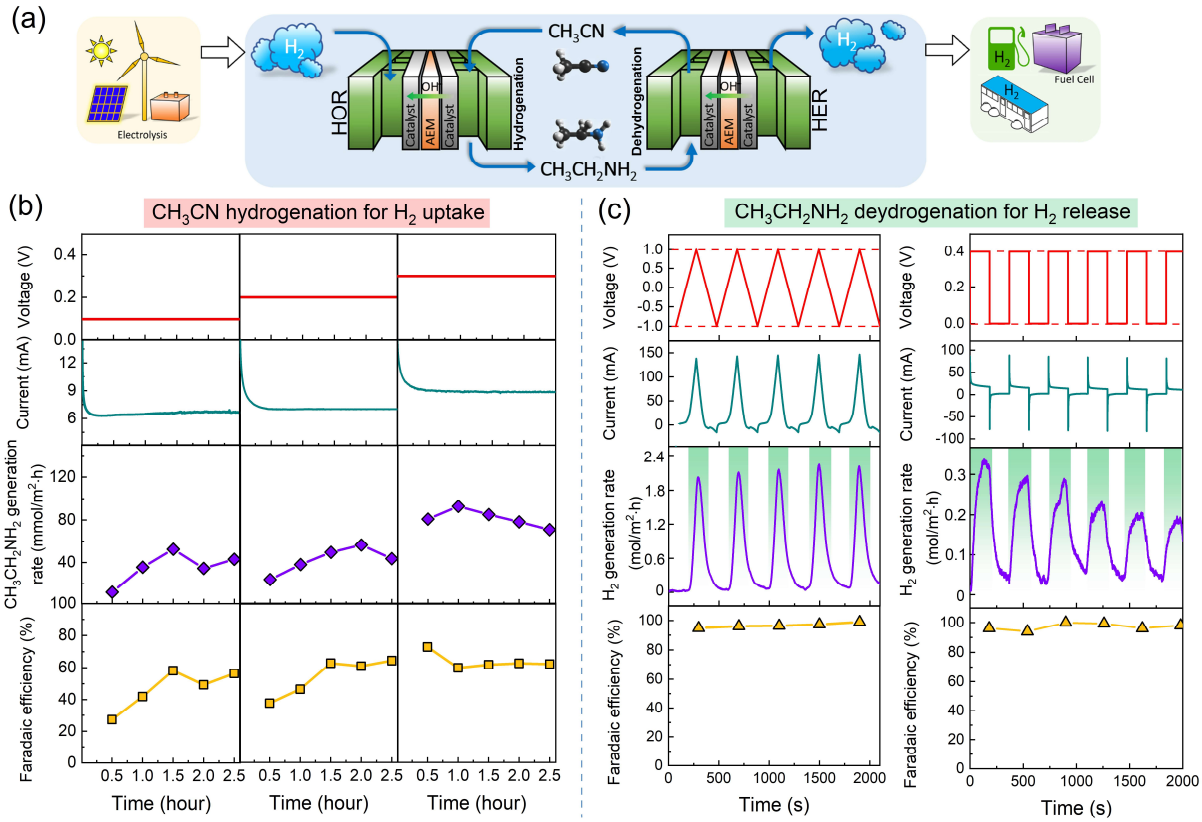

Fig. 2. Hydrogen uptake and release experiments using the electrochemical $CH_3CH_2NH_2/CH_3CN$ redox method in a full-cell system. (a) Schematic drawing of a full-cell system that realizes a complete cycle of hydrogen storage under ambient conditions by coupling the electrochemical $CH_3CH_2NH_2/CH_3CN$ redox method with HER/HOR, with hydrogen production from renewable energy and hydrogen applications included to illustrate the sustainable hydrogen economy; (b) Chronoamperometry of CH_3CN hydrogenation for H_2 uptake at different cell voltage, and the measured $CH_3CH_2NH_2$ generation rate and faradaic efficiency; (c) Cyclic voltammetry and on-and-off chronoamperometry of $CH_3CH_2NH_2$ dehydrogenation for

H_2 release, and the measured H_2 generation rate and faradaic efficiency under the testing conditions.

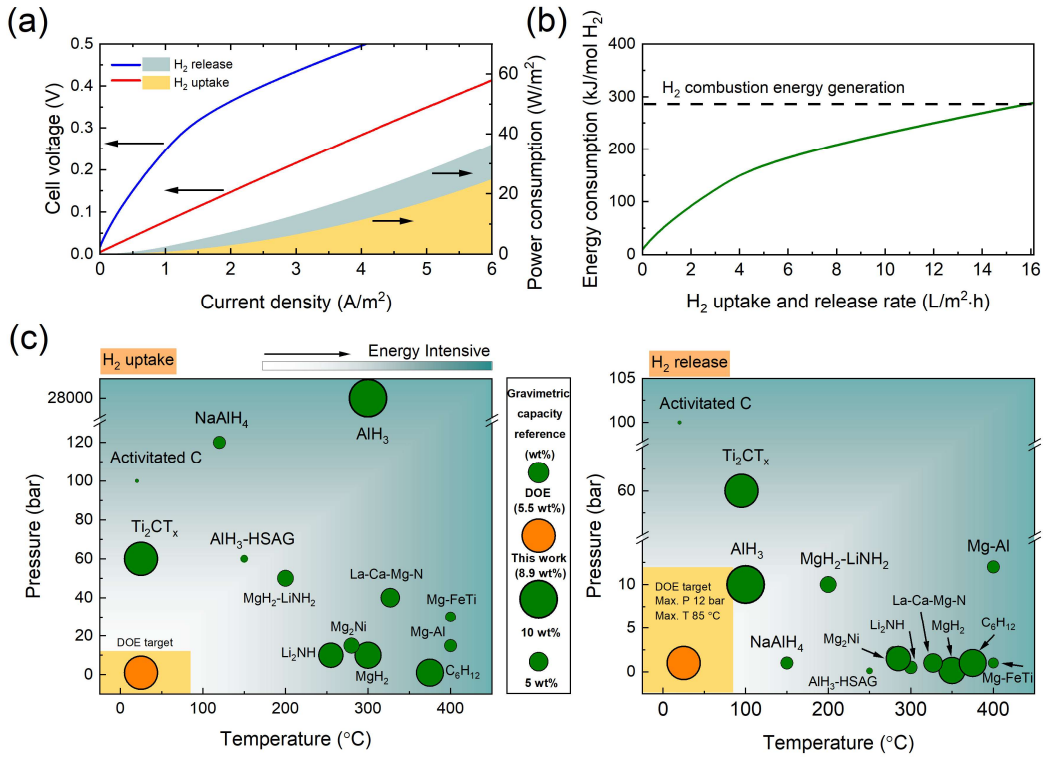

Fig. 3. Energy consumption analysis of the electrochemical $CH_3CH_2NH_2/CH_3CN$ redox method for hydrogen storage and its technical advantages compared with literature studies. (a) Full-cell I-V curves for H_2 uptake and release steps, and corresponding power consumption; (b) Calculated energy consumption for completing a complete hydrogen storage cycle as a function of H_2 uptake and release rate; (c) Comparison of the electrochemical $CH_3CH_2NH_2/CH_3CN$ redox method with literature data of other reported methods in terms of hydrogen storage capacity, operation pressure and temperature.